To be published in Optics Letters:

Title: Full image reconstruction in frequency-domain photoacoustic microscopy by means of a low-cost I/Q demodulator

Authors: George Tserevelakis,Konstantinos Mavrakis,Nikitas Kakakios,Giannis Zacharakis

Accepted: 22 August 21

Posted 25 August 21

DOI: https://doi.org/10.1364/OL.435146

Full image reconstruction in frequency-domain photoacoustic microscopy by means of a low-cost I/Q demodulator

GEORGE J. TSEREVELAKIS, KOSTAS G. MAVRAKIS, NIKITAS KAKAKIOS, GIANNIS ZACHARAKIS*

Institute of Electronic Structure and Laser, Foundation for Research and Technology Hellas, Heraklion, Crete, Greece
**Corresponding author: zahari@iesl.forth.gr*

Received XX Month XXXX; revised XX Month, XXXX; accepted XX Month XXXX; posted XX Month XXXX (Doc. ID XXXXX); published XX Month XXXX

We present a full image reconstruction methodology in frequency-domain photoacoustic microscopy using a low-cost I/Q demodulator for the recording of amplitude and phase of the signals. By modulating the intensity of a continuous wave diode laser at 10 MHz, we have been able to provide accurate optical absorption images and surface reconstructions of phantom samples, comparing also the extracted results with standard time-domain approaches. The findings of this study could be utilized towards the development of inexpensive photoacoustic microscopes with multispectral capabilities for a wide range of biomedical studies, requiring the sensitive detection of endogenous or exogenous absorbers in tissues.

Biomedical photoacoustic (PA) microscopy is a powerful diagnostic technique providing optical absorption contrast from several biomolecules including hemoglobin and melanin, with high spatial resolution and increased penetration depths compared to conventional light microscopy approaches [1]. These capabilities have been recently utilized in several applications involving the *in-vivo* acquisition of valuable anatomical, molecular, functional, and flow dynamic information, towards the understanding of fundamental biological mechanisms such as cancer formation and growth [2]. For an efficient signal excitation, typical PA microscopes usually integrate expensive Q-switched pulsed laser sources emitting at a small number of wavelengths, limiting thus the applicability of the imaging method. In such a case, PA signal is detected in the time-domain (TD), requiring high-speed data acquisition with rates of several hundreds of MSamples/sec, which increases additionally the microscope's total budget. Therefore, in order to expand further the rich potential of PA microscopy in biomedical research, it is necessary to reduce drastically the cost of respective PA systems, improving also their multispectral imaging capabilities. Within this framework, emphasis has been lately given to the development of low-cost PA imaging devices integrating diode lasers, and implemented both in TD (through the generation of short light pulses) [3,4] and frequency-domain (FD), using a sinusoidal modulation of optical intensity [5,6]. Lock-in detection is quite common in FD imaging systems, offering high sensitivity in the recording of PA signals, however, such a solution is also rather expensive, especially when the required bandwidth is in the order of several MHz. A previous study [7], demonstrated the potential of a low-cost I/Q demodulation device incorporated in a FD PA microscope, by recording multiple scans at a range of different discrete frequencies. The final PA reconstruction was generated following the simple summation of the individually acquired images, resulting in an approximate optical absorption map of the sample. Nevertheless, this approach is relatively slow and has not provided any depth information of the imaged absorbers. In this letter, we present a full image reconstruction methodology in optical resolution FD PA microscopy by employing a low-cost I/Q demodulator under single-frequency excitation conditions.

The FD PA microscope (Fig. 1) integrates a continuous wave (CW) diode laser emitting visible radiation at wavelength λ = 488 nm (MDL-III-488, CNI, Changchun, China; maximum power output: 100 mW). A positive lens (L1; focal distance: 15 cm) focuses the beam on the active aperture of a free-space acousto-optic modulator (AOM; TEM-200-50, Brimrose, Maryland, USA; modulation bandwidth: 50 MHz), temporally modulating the instantaneous intensity of radiation with high efficiency. For analog modulation, the acousto-optic driver requires the input of a sinusoidal voltage (selected frequency: 10 MHz; range: 0-1 V), which is provided by an arbitrary function generator (FG; DG5252, Rigol, Oregon, USA; max frequency: 250 MHz). The modulated light is collimated using a second positive lens (L2; focal distance: 15 cm) and subsequently filtered through a small aperture of 5 mm in diameter to isolate exclusively the first order of the resulting diffraction pattern. The filtered radiation is guided on a galvanometric scanner (GM; Scancube 7, Scanlab, Puchheim, Germany), which raster scans the laser beam across the sample to

achieve a fast image acquisition. An optical telescope consisted of two positive lenses (L3; focal distance: 7.5 cm; L4; focal distance: 17.5 cm) is further employed for sufficient beam expansion (~2.3 X), prior the reflection of radiation into a properly modified inverted optical microscope (Diaphot, Nikon, Tokyo, Japan). An objective lens (Obj; Achromat 8X, LOMO, St. Petersburg, Russia; numerical aperture (NA): 0.2) focuses the light on the sample (S), which is placed at the bottom of an optically transparent water tank (WT) and firmly fixed using a thin layer of ultrasound gel. The generated PA waves are detected by a spherically focused piezoelectric ultrasonic transducer (UT; V373-SU, Olympus, Tokyo, Japan; nominal central frequency: 20 MHz; -6 dB bandwidth: 13.3–32.9 MHz, focal distance: 31.3 mm), which is fixed on a system of high-resolution manual XYZ translational stages (PT3, Thorlabs, New Jersey, USA) and immersed into the water tank in a slightly out of focus position with respect to the optical focus for field of view extension.

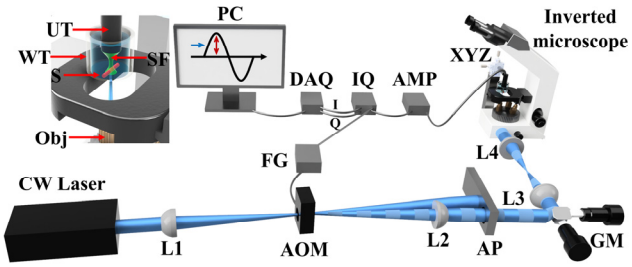

Fig. 1. Three-dimensional illustration of the FD PA microscope. Inset shows a close-up view of the excitation and detection configuration in the microscope. Abbreviations: L1-L4: Positive lenses; AOM: Acousto-optic modulator; AP: Aperture; FG: Function generator; GM: Galvanometric scanner; XYZ: Manual translational stages; AMP: amplifier; IQ: I/Q demodulator; DAQ: Data acquisition card; PC: Recording computer; UT: Ultrasonic transducer; SF: Sensitivity field; WT: Water tank; S: Sample; Obj: Objective lens.

The distilled water in the tank serves as a coupling medium between the signal source and the transducer, ensuring the efficient propagation and detection of PA waves. The generated signals are enhanced by two low-noise RF amplifiers (AMP; TB-414-8A+, Mini-Circuits, Camberley, England; gain: 31 dB) connected in series to provide a total gain of 62 dB, prior their transmission in an I/Q demodulator (IQ; AD8333, Analog Devices, Massachusetts, USA; bandwidth: DC to 50 MHz). The demodulator additionally receives a 4X local oscillator signal at 40 MHz from a second channel of the function generator to provide I and Q values which are recorded and stored by a data acquisition card (DAQ; PCIe-6363, National Instruments, Texas, USA; maximum sampling rate: 2 MS/s) and a computer in synchronization with the galvanometric scanner. The I and Q values are directly used to estimate the amplitude (Amp) and phase (Ph) of the PA signal through the equations $Amp = \sqrt{I^2 + Q^2}$ and $Ph = tan^{-1}\left(\frac{Q}{I}\right)$ respectively. To enhance the signal to noise ratio levels, a total number of 4000 measurements is averaged for the extraction of the I/Q values resulting in amplitude and phase calculation. The typical average power on the sample's plane has been measured at 7 mW, ensuring that no photodamage effects are observed during the imaging procedures. Control and synchronization of the microscope has been performed using custom-developed programs. Finally, all recorded data have been processed by means of MATLAB programming environment and ImageJ open-source Java-based software.

We have initially investigated the amplitude and phase dependence on the relative distance between the optical focus and ultrasonic transducer, using a black tape sample for the efficient generation of PA signals. A series of amplitude and phase measurements was conducted by gradually approaching the transducer towards the PA signal source using the Z-axis translational stage. Fig. 2(a) shows the PA amplitude measurements recorded by covering a total vertical displacement of 430 μm at 10 μm steps. The data points were further fitted by a sine function (R^2 = 0.987) having the typical form

$$y = y_0 + Asin(kx + \varphi) \qquad (1)$$

to estimate the PA amplitude offset (y_0 = 7.294 mV), the maximum absolute difference between PA amplitude and offset (A = 1.502 mV), the wavenumber parameter (k = 4.254 x 10^{-2} μm^{-1}), and an initial phase (φ = -219.9 deg). Furthermore, a characteristic wavelength of the observed oscillation was calculated as λ = 2π / k, to provide a value equal to 147.7 μm, which corresponds with high accuracy to the acoustic wavelength in distilled water for the employed 10 MHz excitation frequency (148 μm at 20 °C) [8]. This oscillatory behavior of the PA amplitude as a function of the detector's vertical position can be physically explained in terms of PA signal's interference across the transducer's finite surface. In other words, the approximately spherical PA wavefront interacts with the transducer's surface at slightly different times, resulting in a cumulative response which depends on the local interference conditions and thus, the relative distance between the signal source and the detector. This interpretation is further supported by the fact that the amplitude oscillation repeats itself following a vertical displacement equal to the corresponding acoustic wavelength, as it should be observed in the case of wave interference. However, PA microscopy images require that the recorded amplitude is independent of the detector's arbitrary relative position, and should be proportional exclusively to the local optical absorption properties of the sample. In this direction, the apparent PA amplitude ambiguity can be eliminated through the recording of an additional 90 degrees phase-shifted measurement, by directly providing a respective phase value in the modulation voltage of the acousto-optic device. Under such circumstances and by using the previous fitting equation Eq. (1), the optical absorption magnitude dependent parameter A can be estimated through the relation

$$A = \sqrt{(y_{0deg} - y_0)^2 + (y_{90deg} - y_0)^2} \qquad (2)$$

where y_{0deg} and y_{90deg} represent the amplitude measurements at 0 and 90 degrees, which are recorded for a constant vertical position of the transducer. On the other hand, Fig. 2(b) presents the simultaneously acquired phase measurements, similarly fitted with a sine function (R^2 = 0.940) to provide a respective PA phase offset (y_{0pha}= -116 deg), the maximum absolute difference between the recorded PA phase and offset (A_{pha} = 10.74 deg), the wavenumber parameter k_{pha} = 4.178 x 10^{-2} μm^{-1}, as well as, an initial phase parameter (φ_{pha} = 59.6 deg). Contrary to the expected 360 degrees phase range of the PA wave as a function of the transducer's vertical distance, the ultrasonic detector demonstrates a limited variability approximating 21.5 degrees, which results from a phase averaging effect across the transducer's surface, in correspondence to the previously shown PA amplitude measurements. The fitting parameters of the phase data points, were subsequently employed for the generation of a calibration curve having a typical inverse sine

form (Fig. 2(c)). The graph provides without ambiguity, the relative depth of PA signal generation as a function of the recorded phase in a range equal to half acoustic wavelength. This means that if the spatial features of the sample in the axial direction present a variability which is larger than ~74 μm, there will be an uncertainty in the determination of the PA signal's depth, at least in the case of a single modulation frequency.

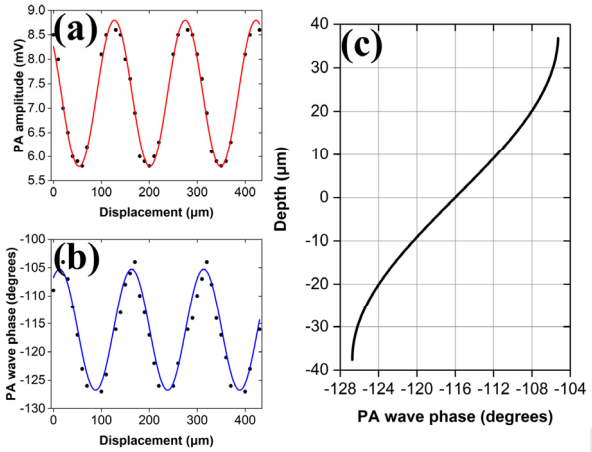

Fig. 2. (a) PA amplitude measurements as a function of relative distance from the detector. Red curve corresponds to a sine fitting of data points. (b) Similar measurements of PA phase fitted with a sine function (blue curve). (c) Inverse sine curve providing the relative depth of PA signal as a function of the detected phase, as generated from the sine fitting shown in (b).

Having investigated the PA signal behavior during spot measurements, we proceeded to the imaging of a black pigmented, cylindrical plastic phantom sample with a diameter in the order of 200 μm. For this imaging session, we purposely underfilled the back aperture of the objective lens, achieving a reduced NA of ~0.1 (optical intensity on the sample: 4.96×10^4 W/cm^2) and a respective depth of focus at ~50 μm (given by the ratio λ/NA^2), which is directly comparable to the maximum range of accurate depth determination. Fig. 3(a) presents an amplitude image in green color scale depicting a part of the phantom, by scanning a region of 520 by 520 μm^2, which is sampled using 200 by 200 pixels. A sequential amplitude image recorded at 90 degrees phase shift in comparison to Fig. 3a is shown in Fig. 3b (red color scale), revealing a different contrast distribution due to the apparent sinusoidal modulation of PA signal. By combining the two previous amplitude images through Eq. (2), we generated a full PA amplitude reconstruction (Fig. 3(c)), representing the optical absorption properties of the sample. Signal variations across the surface can be attributed to possible interference of PA waves with back reflections arising from the glass substrate of the water tank. A PA phase map is additionally presented in Fig. 3(d), to demonstrate the full range of detected phases (±10.74 degrees) in the cylindrical phantom. Aiming to provide an accurate surface reconstruction, we have unfolded in space the full amplitude image of Fig. 3(c) according to the respective phase map and calibration curve shown in Fig. 2(c). The image processing result is demonstrated in Fig. 4(a), uncovering the half of phantom's cylindrical surface with adequate spatial resolution.

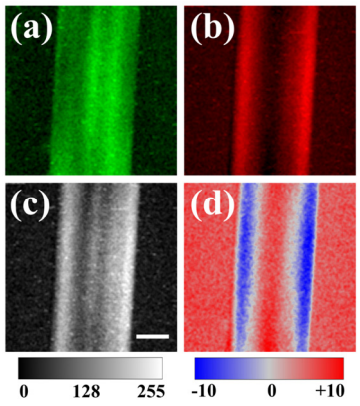

Fig. 3. (a) PA amplitude image of a plastic cylindrical phantom at 0 degrees. (b) Respective amplitude image recorded at 90 degrees phase shift. (c) Full amplitude reconstruction of the phantom. Values below the grayscale bar represent 8-bit pixel brightness. Scalebar is equal to 100 μm. (d) Simultaneously recorded phase image. Numbers below the color-bar represent phase values in degrees.

A XZ profile of the reconstruction is additionally presented in Fig. 4(b) to highlight the accuracy of the proposed approach as regards the determination of PA signal's depth within a specific range, revealing also the expected artifacts at phantom's borders (diagonal lines connecting the sample with the reference plane), as a result of phase ambiguity. In order to validate further the proposed reconstruction methodology, we have additionally imaged the phantom sample using a standard TD optical resolution PA microscope [9,10] which integrated the same objective lens and ultrasonic transducer for signal detection. In this case, each recorded PA waveform was processed by calculating the modulus of its Hilbert transformation, to determine the time point which corresponded to the respective maximum value. The time-of-flight measurements were then translated into depths across the phantom by taking into account the speed of sound in distilled water (1480 m/sec) [8]. Fig. 4(c) shows the TD PA imaging of the half cylindrical surface (scanning step: 2.5 μm; pulse energy: 200 nJ; 20 averages per point), which is directly comparable to the respective FD reconstruction presented in Fig. 4(a). Furthermore, a XZ profile of the phantom as generated through the relative delays of the TD PA signals is presented in Fig. 4(d), verifying the high spatial precision of the FD microscopy surface images.

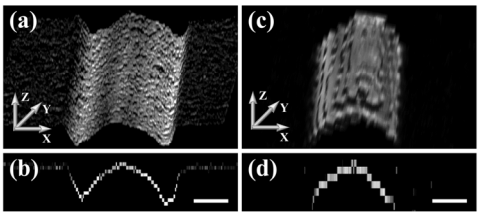

Fig. 4. (a) Surface reconstruction of the cylindrical phantom through amplitude and phase recordings in the FD microscope. (b) Typical XZ profile of the reconstruction shown in (a). (c) Respective surface reconstruction using time of flight measurements in a TD PA microscope. (d) XZ profile of the reconstruction shown in (c). Z-axis is slightly exaggerated in both profiles for improved visualization. Scalebars are equal to 100 μm.

The cylindrical phantom measurements demonstrated the full reconstruction capabilities of the FD microscope using a single modulation frequency at 10 MHz, but also showed the potential artifacts that can appear for a depth variability which is larger than half acoustic wavelength. An effective way to compensate for such an issue, is to drastically restrict the PA excitation region in the axial dimension by increasing adequately the NA of the focusing lens. By filling the back aperture of the objective, the full NA of 0.2 can be exploited (optical intensity on the sample: 1.98×10^5 W/cm^2) to provide a respective depth of focus at ~12 μm, which is more than 6 times smaller than the maximum depth range that can be reconstructed through phase measurements without any ambiguity. Using these new excitation parameters, we have proceeded to the imaging of a black suture sample made of polyester, having a width of ~200 μm. Fig. 5(a) shows a PA amplitude image of the suture (green color scale) recorded at 0 degrees, whereas Fig. 5(b) depicts the respective image at 90 degrees phase shift (red color scale). The two images provide spatial information of different suture regions as a result of the apparent depth variation across its surface, however, none of the single scans is able to provide a faithful optical absorption map of the sample. The full reconstruction of the suture incorporating the two amplitude images through Eq. (2), is explicitly presented in Fig. 5(c), to delineate its internal structure with high resolution and homogeneous contrast. In a similar fashion to the imaging of the cylindrical phantom (Fig. 4), the full PA amplitude image is unfolded in space according to the simultaneously recorded phase map, to generate a surface reconstruction of the sample (Fig. 5(d)) without any depth uncertainty, as a result of the tight beam focusing.

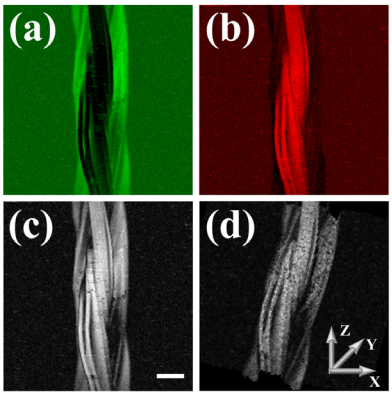

Fig. 5. (a) PA amplitude image of a black suture at 0 degrees. (b) Respective amplitude image recorded at 90 degrees phase shift. (c) Full amplitude reconstruction of the suture. Scalebar is equal to 100 μm. (d) Surface reconstruction of the suture through amplitude and phase measurements.

In conclusion, we have demonstrated the full reconstruction capabilities of a FD PA microscope operating at a single frequency of 10 MHz, through the integration of an I/Q demodulator which provided directly the amplitude and phase of the signals. It is estimated that the total budget required for the development of the presented imaging device could be lower than 25K euros. The lateral resolution of the microscope is ultimately limited by the diffraction of optical radiation, whereas the depth resolution is associated to the demodulator's maximum phase accuracy, provided that the signal to noise ratio is sufficiently high. In this fashion, the FD microscope can reveal spatial details which are much finer than the corresponding acoustic wavelength in the immersion medium. The phase ambiguity issue leading to reconstruction artifacts can be eliminated either by the tight focusing of the beam, which restricts though the effective depth of field, or by recording additional scans at different modulation frequencies (e.g., 20 MHz) to extend the range of accurate depth determination. However, the additional scans may significantly slow down the imaging process and make it prone to different artifact types such as sample displacement, photodamage effects due to high energy deposition, phase shifts during modulation frequency changes etc. The current setup could be upgraded by adding a second laser source to offer spectral unmixing capabilities through concurrent PA excitation using a distinct modulation frequency per each wavelength. Such an implementation is anticipated to contribute further in the development of low-cost and robust PA microscopes, which will be highly suitable for a wide range of biomedical studies requiring the accurate detection of various absorbers in soft tissues.

Funding. H2020 Laserlab Europe [EC-GA 871124], H2020 FETOPEN project "Dynamic" [EC-GA 863203], BIOIMAGING-GR [MIS 5002755], HELLAS CH [MIS 5002735], INNOVAPROTECT [MIS 5030524].

Acknowledgments. G.J.T would like to thank Mr. Andreas Lemonis for his valuable support in the development of the PA microscope.

Disclosures. The authors declare no conflicts of interest.

Data availability. No data were generated or analyzed in the presented research.

References

1. V. Ntziachristos, "Going deeper than microscopy: the optical imaging frontier in biology," Nat. Methods **7**, 603–614 (2010).
2. S. Jeon, J. Kim, D. Lee, J.W. Baik, C. Kim, "Review on practical photoacoustic microscopy," Photoacoustics **15**, art. no. 100141A (2019).
3. Stylogiannis, L. Prade, A. Buehler, J. Aguirre, G. Sergiadis, and V. Ntziachristos, "Continuous wave laser diodes enable fast optoacoustic imaging," Photoacoustics **9**, 31-38 (2018).
4. R.G. Kolkman, W. Steenbergen, and T.G. van Leeuwen, "In vivo photoacoustic imaging of blood vessels with a pulsed laser diode," Lasers Med Sci. **21(3)**, 134-9 (2006).
5. G. Langer, B. Buchegger, J. Jacak, T.A. Klar, and T. Berer, "Frequency domain photoacoustic and fluorescence microscopy," Biomed Opt Express. **7(7)**, 2692-702 (2016).
6. D. George, H. Lloyd, R.H. Silverman, and P.V. Chitnis, "A frequency-domain non-contact photoacoustic microscope based on an adaptive interferometer," J Biophotonics **11(6)**, e201700278 (2018).
7. S. Kellnberger, D. Soliman, G.J. Tserevelakis, et al., "Optoacoustic microscopy at multiple discrete frequencies," Light Sci Appl **7**, 109 (2018).
8. S.J. Kleis, and L.A. Sanchez, "Dependence of speed of sound on salinity and temperature in concentrated NaCl solutions," Sol. Energy **45(4)**, 201–206 (1990).
9. G.J. Tserevelakis, M. Tsagkaraki, and G. Zacharakis, "Hybrid photoacoustic and optical imaging of pigments in vegetative tissues," J. Microsc. **263(3)**, 300-306 (2016).
10. G.J. Tserevelakis, K. G. Mavrakis, D. Pantazopoulou, E. Lagoudaki, E. Detorakis, and G. Zacharakis, "Hybrid autofluorescence and photoacoustic label-free microscopy for the investigation and identification of malignancies in ocular biopsies," Opt. Lett. **45(20)**, 5748-5751 (2020).